Orbital trajectory of an acoustic bubble in a cylindrical resonator

Cyril Desjouy,* Pauline Labelle, Bruno Gilles, Jean-Christophe Bera, and Claude Inserra
INSERM, U1032, LabTAU, Université Claude Bernard Lyon 1, 151 Cours Albert Thomas, 69003, Lyon, France
(Received 21 February 2013; published 9 September 2013)

Acoustic cavitation-induced microbubbles in a cylindrical resonator filled with water tend to concentrate into ring patterns due to the cylindrical geometry of the system. The shape of these ring patterns is directly linked to the Bjerknes force distribution in the resonator. Experimental observations showed that cavitation bubbles located in the vicinity of this ring may exhibit a spiraling behavior around the pressure nodal line. This spiraling phenomenon is numerically studied, the conditions for which a single cavitation bubble follows an orbital trajectory are established, and the influences of the acoustic pressure amplitude and the initial bubble radius are investigated.

DOI: 10.1103/PhysRevE.88.033006 PACS number(s): 47.55.dd

I. INTRODUCTION

A gas bubble in a liquid may exhibit different motions depending on the involved forces: zigzagging and spiraling motions due to hydrodynamic forces when bubbles rise through a liquid [1], motions towards an acoustic pressure node or antinode due to the primary Bjerknes force [2], or spiraling motions when acoustic and hydrodynamic forces compete [3]. In the case where the only force is the acoustic force, most of the experimental and numerical studies focus on the radial oscillations of bubbles. Marmottant *et al*. showed that these radial oscillations give rise to microstreamlines in the surrounding fluid that can conduct to controlled deformations, motions, and rupture of nearby vesicles [4], opening applications in a diverse range of engineering and biomedical fields such as particle trapping and transport [5,6], mixing [7], or cell sonoporation [8]. Although most of these applications involve space displacements of the cavitation bubbles, the translational bubble motions are still much less studied than the radial bubble dynamics. In the 1970s, Miller [9] observed bubbles moving to particular locations and organizing into stable arrays in a standing-wave acoustic field. He also noticed that, depending on their sizes, these bubbles may be trapped or experience orbital trajectories in the vicinity of the pressure node locations. In the analysis of this phenomenon, Miller did not consider the bubble radial dynamics, but a more recent study by Doinikov *et al*. [10] showed that the coupling between the radial oscillations and the translational motions of a spherical bubble in a strong acoustic field can result in translational instabilities of the bubble around a pressure nodal plane. Even if understanding the traveling or dancing motions of a bubble is a key to provide further insight into bubble control, no particular attention was paid to the translational motions that bubbles could exhibit in a complex and realistic three-dimensional acoustic field. The aim of this paper is to investigate the behavior of bubbles in a cylindrical ultrasonic standing wave. Supported by preliminary experimental observations, theoretical and numerical studies are conducted to determine how bubbles can concentrate into specific patterns in a cylindrical geometry, and particularly which behavior a single bubble located on (or in the vicinity of) this pattern can exhibit depending on the modal distribution of the acoustic field, the initial radius of the bubble, and the acoustic pressure amplitude.

II. RINGING AND SPIRALING BUBBLE OBSERVATIONS

A 30 kHz continuous acoustic wave is generated in a cylindrical resonator of inner radius $a = 4.0 \times 10^{-2}$ m filled up to a fixed position $h = 4.8 \times 10^{-2}$ m with air-saturated spring water at standard conditions of temperature T_0 and pressure P_0, using a plane ultrasonic transducer with an active diameter of 7.9×10^{-2} m, which is located at $z = 0$. The spacial distribution of the acoustic pressure amplitude P_a in the medium is measured with a hydrophone (Reson TC4034). This amplitude can be adjusted from 0–8 bar at the pressure antinode. The measurement of the displacements of the ultrasound-induced microbubbles is carried out with a high-speed camera (Vision Research Phantom v12.1). At moderate pressure amplitudes ($0.5 < P_a < 2.5$ bar), the cavitation-induced bubbles concentrate into ring patterns [Fig. 1(a)], located at pressure nodes, and made by bubbles whose radii vary around the equilibrium radius, from 70–120 μm. The radius of the bubble ring is of about 2.5×10^{-2} m whatever the value of the pressure amplitude. Some of the bubbles located on this ring exhibit particular dynamics: they follow an orbital path around the pressure nodal line. This behavior in the (r, z) plane is illustrated in Fig. 1(b) showing bubbles spiraling in the vicinity of the ring pattern. Figure 1(c) presents the r and z displacements of a spiraling bubble as a function of time t. The two components of the displacement are sinusoidal. In this example, the phase between these components nearly equals $\pi/2$ and peak-to-peak amplitudes of the r and z displacements are both of about 2 mm, so that the bubble describes a quasicircular trajectory with a constant radius $R_p \simeq 1.0 \times 10^{-3}$ m and a center located on a pressure nodal line, i.e., here at $r_c \simeq 2.5 \times 10^{-2}$ m.

III. THEORETICAL BACKGROUND

The bubble ring structure is directly linked to the acoustic waveform in the resonator. Indeed, assuming that the acoustic field is stationary and azimuthally symmetric, the complex acoustic pressure $\tilde{p}_a$ in a cylindrical closed ends resonator can classically be expressed in the cylindrical coordinate system

*cyril.desjouy@inserm.fr

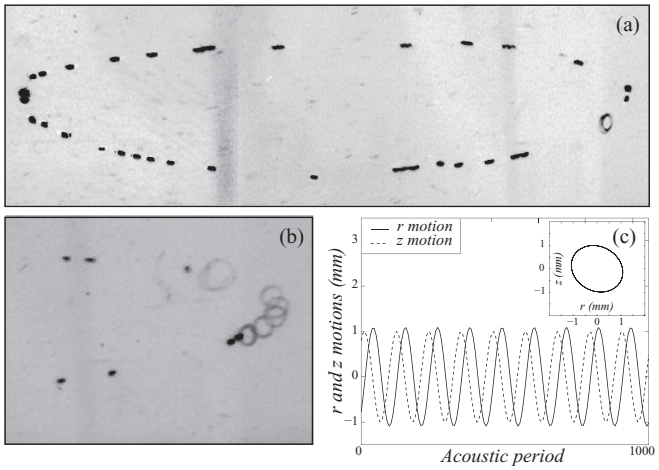

FIG. 1. View of (a) a bubble ring, (b) spiraling bubbles, and (c) r and z displacements of a spiraling bubble. Insert: bubble trajectory in the (r, z) plane. $P_a \simeq 1.5$ bar.

(r,θ,z) as

$$\tilde{p}_a = P_a \sum_{\nu=0}^{\infty}\sum_{m=0}^{\infty} \tilde{A}_{\nu,m} J_\nu\left(k_{w_{\nu,m}} r\right) \cos\left(k_{z_{\nu,m}} z\right) e^{i\omega t}, \qquad (1)$$

where $\tilde{A}_{\nu,m} = A_{\nu,m} e^{i\phi_{\nu,m}}$ is the modal complex amplitude of the mode (ν,m), ω is the driving angular frequency, J_ν is the cylindrical Bessel function of νth order, $k_{w_{\nu,m}}$ (determined thanks to the boundary condition at $r = a$) and $k_{z_{\nu,m}}$ are the radial and longitudinal wave numbers, which satisfy the dispersion equation $k^2_{w_{\nu,m}} + k^2_{z_{\nu,m}} = \omega^2/c^2$, c being the adiabatic celerity of sound in the medium. At the experimental driving frequency (i.e., $f = \omega/2\pi = 30$ kHz), the two symmetric modes (0,0) and (0,1) propagate into the resonator. Other modes are antisymmetric or evanescent. It is worth noting that the longitudinal closed ends boundary condition chosen in this model does not reflect the realistic complex conditions at $z = 0$ (transducer surface deformation) and $z = h$ (free surface deformation). The fact is that taking into account a simplified closed ends condition does not affect the number of modes that propagate into the resonator but only the z location of the pressure nodes and antinodes, and, as a consequence, the z locations of the bubble patterns, which are not of interest here.

Assuming that the energy transfers involved at the longitudinal boundaries and through the acoustic scattering due to the presence of bubbles ensure that the total energy of the system

$$E = \int_V \rho \frac{\tilde{\boldsymbol{v}}_{\boldsymbol{a}}^{\boldsymbol{2}}}{2} dV + \int_V \frac{\tilde{p}_a^2}{2\rho c} dV, \qquad (2)$$

where ρ is the density of fluid, $\tilde{v}_a$ is the acoustic velocity, and V denotes the volume of the system, is divided in equal parts between the two modes constituting the acoustic field in the resonator. The principle of equipartition of the energy [11] can be applied as follows:

$$\langle E_{0,0}\rangle = \langle E_{0,1}\rangle, \qquad (3)$$

where $\langle E_{\nu,m}\rangle$ is the mean of the energy $E_{\nu,m}$ of the mode (ν,m) over an acoustic period. Writing the relationship between the modal amplitudes $A_{0,0}$ and $A_{0,1}$ as $A_{0,0} + A_{0,1} = 1$, the equation (3) leads to:

$$A_{0,0} = \frac{\alpha}{1+\alpha} \simeq 24.8\%, \qquad (4)$$

where

$$\alpha = J_0(\chi_{1,1}) \sqrt{\frac{2}{\pi}\left(1 + \frac{k^2_{w_{0,1}}}{k^2_{z_{0,0}}} \mathrm{sinc}\left(2k_{z_{0,1}} h\right)\right)}. \qquad (5)$$

As regards modal phases, $\phi_{0,0}$ is set as a reference ($\phi_{0,0} = 0$). Then $\phi_{0,1}$ can be determined assuming that there is a local equilibrium of the energy. This means that the coupling energy vanishes over an acoustic period, which leads, after calculation, to:

$$\phi_{0,1} = \pm\pi/2. \qquad (6)$$

The main force that acts on a single bubble is the well-known primary Bjerknes force written as

$$\boldsymbol{F}_{\boldsymbol{b_1}} = -\frac{4}{3}\pi R^3 \boldsymbol{\nabla} p_a, \qquad (7)$$

where $R(t)$ is the time-dependent radius of the spherical bubble, and where $\boldsymbol{\nabla}$ is the gradient operator. Equations (1) and (7) clearly show the existence of zeros of the Bjerknes force, which take the form of a ring which is a stable (unstable) equilibrium location for bubbles larger (smaller) than the resonant radius at low excitation amplitude [12]. The radius of this ring is given by the first zero $\chi_{1,1}$ of the Bessel function $J_1(k_{w_{0,1}} r)$, which is located at $r = \chi_{1,1}/k_{w_{0,1}} = 2.5 \times 10^{-2}$ m. The value of this theoretical radius coincides with the experimental one. This result clearly explains the formation of a ring pattern made by large bubbles at the pressure nodes in a cylindrical resonator, but does not explain the presence of spiraling bubbles. This spiraling behavior suggests that there is a translational instability that causes the bubble to turn around the nodal line. Some authors have already worked on this kind of instability. In particular, Doinikov [13] extended Watanabe and Kukita's works [14] on the translational motion of a spherical bubble in a standing wave acoustic field. Doinikov rederived the one-dimensional equations of motion of a bubble using an energy approach that enables a feedback between the radial and the translational motions. Then, these two motions can be described in the (r, z) plane by a three equation system as follows:

$$\left(1 - \frac{\dot{R}}{c}\right) R\ddot{R} + \left(\frac{3}{2} - \frac{\dot{R}}{2c}\right)\dot{R}^2 - \frac{1}{\rho}\left(1 + \frac{\dot{R}}{c} + \frac{R}{c} d_t\right)\tilde{p} = \frac{1}{4}\dot{\boldsymbol{r}}^{\boldsymbol{2}}, \qquad (8)$$

$$\ddot{\boldsymbol{r}} + 3\frac{\dot{R}}{R}\dot{\boldsymbol{r}} = \frac{3}{2\pi\rho R^3}\boldsymbol{F}_{\mathbf{ext}}, \qquad (9)$$

where $\boldsymbol{r}$ is the position vector in the (r, z) plane, and where the external force $\boldsymbol{F}_{\mathbf{ext}}$ takes into account the primary Bjerknes force $\boldsymbol{F}_{\boldsymbol{b_1}}$ and the Levich viscous drag [15] as follows:

$$\boldsymbol{F}_{\mathbf{ext}} = \boldsymbol{F}_{\boldsymbol{b_1}} - 12\pi\eta R(\dot{\boldsymbol{r}} - \tilde{\boldsymbol{v}}_{\boldsymbol{a}}). \qquad (10)$$

The scattering pressure $\tilde{p}$, expressed as

$$\tilde{p} = \left(P_0 + \frac{2\sigma}{R_0}\right)\left(\frac{R_0}{R}\right)^{3\gamma} - \frac{2\sigma}{R} - \frac{4\eta\dot{R}}{R} - P_0 - \tilde{p}_a, \qquad (11)$$

where σ is the surface tension of the bubble, R_0, its initial radius, γ, the polytropic exponent, and η, the viscosity of the fluid, takes into account the complete acoustic pressure field defined in Eq. (1).

IV. NUMERICAL MODELING OF THE SPIRALING MOTION

Numerical computations are made using the PYTHON programming language to simulate radial and translational motions of a single spherical bubble in a cylindrical acoustic field. The numerical constants are matched to the experimental ones (i.e., $P_0 = 1020$ hPa, $T_0 = 21\,^{\circ}$C, $\rho = 983$ kg/m^3, $\eta = 1.0.10^{-3}$ kg m^{-1} s^{-1}, $\gamma = 1.4$, and $\sigma = 0.0725$ N/m). Numerical simulations are computed over 2000 acoustic cycles and the initial location of the bubble is set in the vicinity of a pressure node ($r_c \simeq \chi_{1,1}/k_{w_{0,1}}$ and $z_c \simeq 3h/4$). Figures 2(a)–2(d) present the trajectory of a single bubble in the resonator for different values of $A_{0,0}$ and $\phi_{0,1}$. The ratio ω/ω_0, where

$$\omega_0 = \frac{1}{R_0}\left(\frac{3\gamma P_0}{\rho} + \frac{2\sigma(3\gamma - 1)}{\rho R_0}\right)^{1/2} \tag{12}$$

is the linear resonance frequency of a bubble, gives information on the bubble size. Figure 2(a) shows the path described by a bubble for $A_{0,0} = 100\%$. In this case, only the mode (0,0) is considered. This results in unidirectional oscillations of the bubble. When the amplitude $A_{0,0}$ decreases to 25% with $\phi_{0,1} = 0$, [Fig. 2(b)], the bubble oscillates in the (r, z) plane. When $\phi_{0,1}$ equals $\pi/2$, the trajectory of the bubble becomes orbital [Figs. 2(c) and 2(d)]. This trajectory may be elliptic [Fig. 2(c)] or quasicircular [Fig. 2(d)] depending on the $A_{0,0}$ value. In this latter case, the revolution period of the bubble is of about 5 ms, which is of the same order of magnitude as the experimental one [of about 4 ms on Fig. 1(c)]. It is worth noting that the unidirectional [Fig. 2(a)] and erratic [Fig. 2(b)] motions of the bubbles have already been studied in recent works when considering only the mode (0,0) [10] or only the mode (0,1) [16], respectively. The present study highlights that

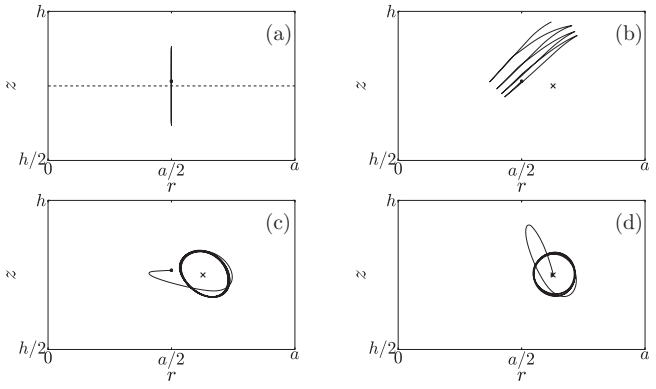

FIG. 2. Trajectory of a bubble in the (r, z) plane for $\omega/\omega_0 = 0.87$ and $P_a = 0.8$ bar, where the dot represents the starting location of the bubble: (a) $A_{0,0} = 100\%$ where the dashed line represents the pressure nodal line, (b) ($A_{0,0} = 25\%$, $\phi_{0,1} = 0$), (c) ($A_{0,0} = 25\%$, $\phi_{0,1} = \pi/2$), and (d) ($A_{0,0} = 28\%$, $\phi_{0,1} = \pi/2$), where the crosses represent the pressure node. Note that for (d), the starting location of the bubble is set to the pressure node.

a bubble can describe an orbital trajectory only if both plane and radial modes are considered and if there is a modal phase shift between these two modes. These observations suggest that there exist specific values of the modal parameters $A_{0,0}$ and $\phi_{0,1}$ allowing a bubble to spiral, opening applications in bubble transport when controlling the surrounding acoustic field. Note that Fig. 2 presents results for small bubbles ($\omega < \omega_0$) for which the (r_c, z_c) location is linearly unstable. As regard large bubbles ($\omega > \omega_0$), they tend to move to the pressure nodes and to describe a spiraling trajectory of infinitesimal radius. These results show that the entire bubble population can be located in the vicinity of the bubble ring (i.e., the pressure node).

In the case $\omega > \omega_0$, a theoretical derivation of the modal parameters that enable this particular motion can be achieved by introducing in Eq. (9) a circular motion solution around an equilibrium location ($r_c = \chi_{1,1}/k_{w_{0,1}}$, $z_c = 3h/4$), which is stable for large bubble radii ($\omega > \omega_0$). The (r, z) motion is considered as $(r_c + R_p \cos\theta, z_c + R_p \sin\theta)$ where $\theta = \Omega t$, Ω being the constant angular velocity. Assuming a low pressure amplitude and taking the average over an acoustic period of the Bjerknes force, a circular motion of the bubble is obtained for

$$A_{0,0} = \frac{k_{w_{0,1}} J_1(\chi_{0,1})}{k_{w_{0,1}} J_1(\chi_{0,1}) + k_{z_{0,0}}} \quad \text{and} \quad \phi_{0,1} = \pm\frac{\pi}{2}. \tag{13}$$

The theoretical values of the modal parameters are $A_{0,0} = 27.6\%$ and $\phi_{0,1} = \pm\pi/2$. The first condition ensures that the contributions of r and z components of the Bjerknes force are the same, and the phase condition ensures that there is a phase quadrature relationship between the z component [mainly supported by the mode (0,0)] and the r one [only supported by the mode (0,1)]. Considering that this result is suitable for a low pressure/large bubble approximation, a parametric study is carried on to obtain the values of the modal parameters for which the path of a single small bubble can be orbital as observed in Fig. 2(d). With that aim, for each set of $(A_{0,0}, \phi_{0,1})$ values, the trajectory of the bubble is compared to the equation of an ellipse. The ratio ϵ of the minor and major radii of the ellipse gives the information on the circularity of the bubble path: When ϵ equals 0, the motion of the bubble is nonexistent or erratic, and when ϵ equals 1, the motion is perfectly circular. For intermediate values, the motion of the bubble is elliptic. Figure 3 presents an example of the variations of this ratio ϵ as a function of the modal parameters $(A_{0,0}, \phi_{0,1})$. There exist two areas for which the trajectory of the bubble is orbital. These two areas are located around the sets of values $A_{0,0} = 28\%$ and $\phi_{0,1} = \pm\pi/2$, which are the same values that are given by Eq. (13) for large bubbles. The theoretical values given in Eqs. (4) and (6) that define the modal distribution of the acoustic field in the resonator are included in the dark areas of Fig. 3. For these theoretical values, the trajectories of the bubbles are elliptic [values not exactly equal to those defined by Eq. (13) in the case of perfectly circular]. Even if the experimental setup does not allow a quantitative comparison of the eccentricity of the trajectories, Fig. 1(c) clearly shows that the experimental trajectory of the bubble is also not perfectly circular.

The modal parameters obtained above ensure a circular or quasicircular motion around the pressure nodal line, either for large or small bubbles. This means that for sufficiently high pressure amplitudes, the oscillatory motion of small bubbles around a linearly unstable location becomes stable, as can be

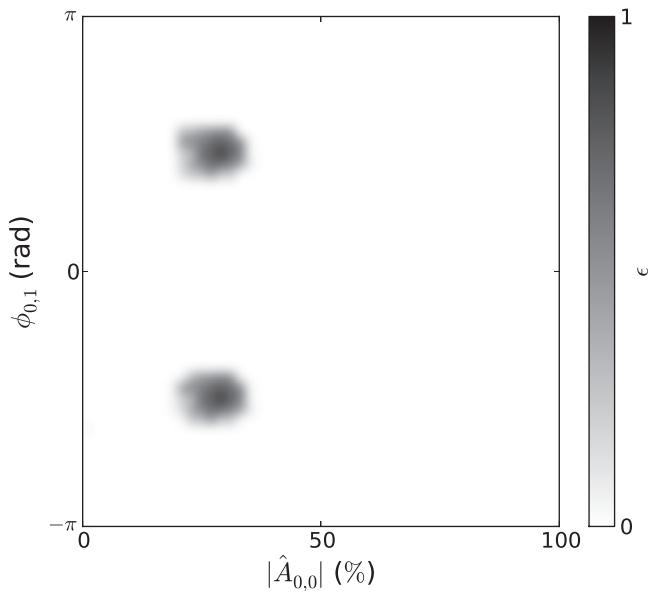

FIG. 3. Example of the variations of the normalized ratio ϵ with respect to the modal parameters $(A_{0,0}, \phi_{0,1})$ for $P_a = 1.5$ bar and $\omega/\omega_0 = 0.87$. Note that numerical simulations provide similar distributions with peaked extrema at the same location whatever the acoustic pressure amplitudes varying from 0.8–2.5 bar.

observed in other contexts of nonlinear oscillator physics [17]. We now investigate the conditions for which stable circular motion of bubbles around the nodal line can be obtained, with $A_{0,0}$ and $\phi_{0,1}$ set to the values obtained above. Figure 4 presents the dependence of the radius R_p of the trajectory of the bubble as a function of ω/ω_0 and P_a. When $\omega > \omega_0$, bubbles experience circular motion around their stable equilibrium location (pressure node). For almost the whole range of the driving pressure amplitudes, circular motions exist with an infinitesimal radius R_p: bubbles are trapped. When $\omega < \omega_0$,

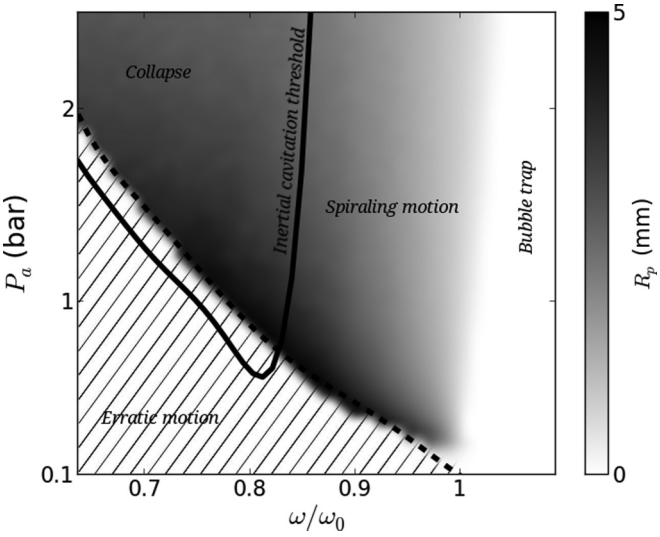

FIG. 4. Trajectory radius R_p as a function of the acoustic pressure amplitude P_a and of the ratio ω/ω_0. The bold continuous line corresponds to the inertial cavitation threshold defined as $R_{\max}/R_0 \simeq 2.3$, $R_{\max}$ being the maximum radius of the bubble.

at low pressure amplitudes (hatched area), bubbles exhibit an erratic motion in the vicinity of their unstable equilibrium location. For sufficiently high pressure amplitudes (above the dashed line), spiraling bubbles exist. Even starting from the unstable location (r_c, z_c), a small bubble stabilizes its motion on a circular path, as illustrated in Fig. 2(d). The pressure threshold for orbital trajectory (dashed line) is intimately linked to the bubble nonlinear dynamics. The continuous line corresponds to the well-known inertial cavitation threshold defined in Ref. [12]. Above this threshold [collapse area, for which Eq. (8) is no longer valid], bubbles collapse preventing them to spiral. Below this threshold (spiraling motion area), cavitation remains stable, even for high pressure amplitudes, due to the coupling between the radial and translational motions. In this area, for a given ω/ω_0 value, increasing the pressure amplitude P_a above the spiraling threshold (dashed line) results in the decrease of the radius R_p, which helps to collect small bubbles in the vicinity of the pressure nodal line. It is worth noting that, for an acoustic pressure amplitude P_a of 1.5 bar, the order of magnitude of the experimental radius R_p [of about 1 mm in Fig. 1(c)] is the same as the one found numerically: from $R_p \simeq 0.8$ mm at $\omega/\omega_0 = 1$ (i.e., close to bubble trap area: $R_0 = 110$ μm) to $R_p \simeq 2.7$ mm at $\omega/\omega_0 = 0.87$ (i.e., close to collapse area: $R_0 = 96$ μm).

V. CONCLUSIONS

Bubbles in a cylindrical resonator can concentrate into ring patterns at the pressure nodes, which correspond to the stable equilibrium location for large bubbles (i.e., with radius larger than R_0). This ring is linked to the acoustic field, which reduces in this geometry to a radial and a longitudinal mode. Under sufficiently high pressure amplitude, the combination of these two modes allows the existence of an orbital trajectory for small bubbles (i.e., with radius smaller than R_0) around the ring pattern, which is their linearly unstable location. This phenomenon may find promising applications in the biomedical and bioengineering areas. Today, the microstreaming induced by acoustic bubbles is widely studied and has already found applications for the enhancement of fluid mixing and transport techniques, which are challenging problems in microfluidic systems. The spiraling phenomenon may help to contribute to these microfluidic problematics. The experimental setup developed here can easily be miniaturized. As an example, for an acoustic system of characteristic dimensions 1.5 mm driven at a frequency of 1 MHz, bubbles can describe an orbital trajectory of radius R_p varying from 0 to 80 μm. Then the combination of a controlled spiraling effect and of the microstreaming generation effect may help to adjust the streamline distributions in microfluidic systems in order to enhance fluid mixing or transport of small objects.

ACKNOWLEDGMENTS

This work is supported by the French National Research Agency ANR project "SonInCaRe", No. 2010-TECS-003-01, and benefits from the Labex CeLyA, No. ANR-10-LABX-0060.

[1] W. L. Shew and J. F. Pinton, Phys. Rev. Lett. **97**, 144508 (2006).
[2] U. Parlitz, R. Mettin, S. Luther, I. Akhatov, M. Voss, and W. Lauterborn, Philos. Trans. R. Soc. London A **357**, 313 (1999).
[3] J. Rensen, D. Bosman, J. Magnaudet, C. D. Ohl, A. Prosperetti, R. Togel, M. Versluis, and D. Lohse, Phys. Rev. Lett. **86**, 4819 (2001).
[4] P. Marmottant and S. Hilgenfeldt, Nature (London) **423**, 153 (2003).
[5] P. Rogers and A. Neild, Lab On Chip **11**, 3710 (2011).
[6] P. H. Jones, E. Stride, and N. Saffari, Appl. Phys. Lett. **89**, 081113 (2006).
[7] D. Amhed, X. L. Mao, J. J. Shi, B. K. Juluri, and T. J. Huang, Lab On Chip **9**, 2738 (2009).
[8] G. N. Sankin, F. Yuan, and P. Zhong, Phys. Rev. Lett. **105**, 078101 (2010).
[9] D. L. Miller, J. Acoust. Soc. Am. **62**, 12 (1976).
[10] R. Mettin and A. A. Doinikov, Appl. Acoust. **70**, 1330 (2009).
[11] A. Snakowska, Acustica **79**, 155 (1993).
[12] T. G. Leighton, *The Acoustic Bubble* (Academic Press, London, 1997).
[13] A. A. Doinikov, Phys. Fluids. **14**, 1420 (2002).
[14] T. Watanabe and Y. Kukita, Phys. Fluids A **5**, 2682 (1993).
[15] B. V. Levich, *Physicochemical Hydrodynamics* (Prentice-Hall, Englewood Cliffs, 1962).
[16] L. A. Kuznetsova, S. Khanna, N. N. Amso, W. T. Coakley, and A. A. Doinikov, J. Acoust. Soc. Am. **117**, 104 (2005).
[17] J. S. Aldridge and A. N. Cleland, Phys. Rev. Lett. **94**, 156403 (2005).